Kinetics of Dye Efflux and Lipid Flip-Flop Induced by δ-Lysin in Phosphatidylcholine Vesicles and the Mechanism of Graded Release by Amphipathic, α-Helical Peptides†

Antje Pokorny and Paulo F. F. Almeida*

Department of Chemistry and Biochemistry, University of North Carolina, Wilmington, North Carolina 28403

Received February 9, 2004; Revised Manuscript Received May 6, 2004

ABSTRACT: δ-Lysin is a 26-residue, amphipathic, α-helical peptide of bacterial origin. Its specificity is to some extent complementary to that of antimicrobial peptides. Therefore, understanding its mechanism is important for the more general goal of understanding the interaction of amphipathic peptides with membranes. In this article, we show that δ-lysin induces graded efflux of the contents of phosphatidylcholine vesicles. In view of this finding, carboxyfluorescein efflux kinetics were re-examined. In addition, peptide-induced lipid flip-flop was directly measured using fluorescence energy transfer between two lipid fluorophores initially placed on opposite leaflets of the bilayer. Carboxyfluorescein efflux and lipid flip-flop occur with essentially identical rate constants. On the basis of a detailed, quantitative analysis of the kinetics of peptide−vesicle interactions, we conclude that the peptide translocates across the bilayer as a small, transient aggregate, most likely a trimer. Dye efflux and lipid flip-flop occur concomitantly with the transient peptide-induced perturbation of the membrane. The experimental data are interpreted by comparing the predictions of the available models for the mechanism of action of amphipathic α-helical peptides. We demonstrate how the combination of the quantitative kinetic analysis, graded efflux, and reversibility of the peptide−vesicle interaction can be used to reject several models for this particular peptide. Two models are compatible with the data, the toroidal pore model and the sinking raft model. On the basis of the small aggregate size, a trimer, the latter appears to be more plausible. Some significant modifications are introduced in the sinking raft model to take into account the new finding of graded dye release. Furthermore, we present an explanation for the phenomenon of graded release in general, which, contrary to all-or-none efflux, has not been well-understood.

As traditional antibiotics have met with increasing acquired bacterial resistance, antimicrobial peptides have received considerable attention as a basis for new alternatives. Many of these peptides form an amphipathic α-helix upon binding to lipid membranes. An understanding of the mechanism of action of these peptides seems to be necessary for the development of improved antibiotics based on a rational design. To do this, we must answer four major questions.

The first question concerns specificity. Antimicrobial peptides produced by higher organisms are not toxic for the cells that produce them. However, very similar peptides are secreted by prokaryotes and are toxic for higher organisms. The family of amphipathic α-helical peptides is quite numerous and has been extensively studied (*1*−*6*), but an examination of the amino acid sequences shows that there is neither a consensus between peptides from different organisms nor a clear distinction between generally toxic and specifically antimicrobial peptides. One of the most studied is magainin-2, an amphibian antimicrobial peptide (*7*), which is specific against prokaryotes. No cell surface receptors appear to be involved in a recognition mechanism because all D-amino acid analogues of magainin-2 are as antimicrobial as the natural all-L form (*8*, *9*). Thus, target cell specificity appears to be determined by the lipid bilayer itself. One of the favored hypotheses is that prokaryotic versus eukaryotic specificity arises because antimicrobial peptides are cationic and bacterial membrane lipids are anionic (*6*, *10*, *11*). In contrast, the lipids of the outer leaflet of eukaryotic membranes are zwitterionic. If charge were the only factor, however, magainin-2 would be equally effective toward lipid membranes of different anionic lipids, but its efficiency in lysing phosphatidylglycerol and phosphatidylserine vesicles differs by 1 order of magnitude (*12*). Furthermore, other cationic peptides, especially the insect venom mastoparans and melittin, are very nonspecific. Thus, although charge certainly plays an important role (*6*), an understanding of the specificity of peptides is still lacking.

The second question concerns the molecular mechanism of vesicle disruption. Several models have been proposed for the structure that is responsible for peptide-induced membrane disruption. We shall call this structure a pore, without necessarily implying that a stable hole is involved. The barrel-stave model (*13*) is the oldest model and borrows from the structure of integral protein ion channels. In this model, the peptide amphipathic helices insert into the membrane and line a water-filled pore (the same way wooden

† This work was supported in part by a Cahill award (University of North Carolina, Wilmington, NC) to P.F.F.A.

* To whom correspondence should be addressed. Telephone: (910) 962-7300. Fax: (910) 962-3013. E-mail: almeidap@uncw.edu.

10.1021/bi0497087 CCC: $27.50
Published on Web 06/10/2004

staves form a barrel). A minimum number of peptides (usually at least 6) is thought to be necessary for formation of a channel. This model has been proposed to account for the action of many peptides, but only alamethicin appears to be consistent with it. It is very questionable for melittin (*14*) and not consistent with experimental data for δ-lysin (*15*). The toroidal hole model (*16*, *17*), first proposed for magainin, states that the peptides remain associated with the phospholipid headgroup region of the bilayer, locally inducing a high-curvature fold in the bilayer, so that the two leaflets of the bilayer communicate directly at a torus lined by the peptides. In contrast with the barrel-stave model, the tori are short-lived, reversibly forming structures, such that, at equilibrium, the peptides are distributed over both leaflets of the bilayer. The carpet model (*5*) proposes that peptides adsorb to the membrane surface until, at a high, critical concentration, they coat the almost entire outer membrane surface of the vesicle, like a carpet. At this point, the peptides work like a detergent, leading to a disintegration of the membrane. The sinking raft model proposes side-by-side aggregation on the membrane, with the peptide helices parallel to the surface, forming a "raft" that sinks into the outer bilayer leaflet (*15*). A sideways insertion was first proposed to explain the conservation of parallel orientation of cecropin A helices relative to the membrane (*18*). As the helices sink deeper into the bilayer, the hydrophobic residues remain in contact with the lipid acyl chains, while the hydrophilic faces of the helices line a hole, in the center of the multimer. The two-state model (*19*) is a "higher-level" model in the sense that it incorporates features of some of the basic models described. It was developed to account for the observation that some peptides, such as the magainins, are surface-adsorbed at low peptide-to-lipid ratios (P/L) and insert into the bilayer at high P/L (*16*, *20*). The model predicts a sharp transition from a surface-adsorbed state (the S-state) to a stable, membrane-inserted state (the I-state) at a critical peptide concentration on the membrane surface. Adsorption of peptides causes bilayer thinning until, when a critical membrane thickness is reached, a concerted peptide insertion occurs, similar to a phase transition.

The third question concerns the mechanism of vesicle leakage. When peptide-induced membrane disruption occurs, leakage of the contents of a lipid vesicle can be graded or all-or-none. That is, if release of an encapsulated dye is not complete, have all vesicles leaked approximately the same amount of dye? Or are there two vesicle populations, one that released almost everything and another that retained its contents? The answer to this question provides valuable information, allowing for a distinction between different models of peptide action, as we will show here.

The fourth question concerns the thermodynamic driving force for peptide-induced membrane disruption. Notwithstanding electrostatic potential-driven insertion in cells, this question needs to be addressed for simple lipid vesicles. In the barrel-stave model, the inserted peptide is presumed to be a low free energy state. In the toroidal and sinking raft models, the driving force is the equilibration of peptide concentrations across the bilayer. In this case, how do the peptides overcome the high free energy state that is represented by the pore? For example, the human antimicrobial peptide LL-37 has been proposed to induce curvature strain and cross the bilayer via the torus model (*21*). But for the cationic peptide penetratin (*22*), which consists of a helix derived from a transcription factor, it has been argued that the charge imbalance resulting from peptide binding to the membrane provides the energy needed to translocate across the bilayer.

A distinction between these models has been sought in structural studies but also by the analysis of dye efflux kinetics from lipid vesicles. However, only very rarely have the models been confronted quantitatively. There have been a few rare instances of approximate solutions of models with quantitative comparison with experiments (*23*, *24*), but most studies used only semiquantitative or qualitative tests. In this article, we address the three last questions using the peptide δ-lysin, secreted by *Staphylococcus aureus*. δ-Lysin is a 26-amino acid residue, hemolytic peptide with no net charge at neutral pH (*25*−*28*). The peptide is largely unstructured, at low concentrations, in aqueous solutions, while adopting an amphipathic α-helical conformation at high concentrations in aqueous solution, in organic solvents, and when bound to micelles or lipid membranes (*29*−*31*). Several biophysical techniques were used to characterize the interaction of δ-lysin with multilamellar vesicles (MLV)[1] (*32*). Molecular modeling and the observation of voltage-dependent channels in phospholipid bilayers (*33*) suggested that δ-lysin forms a hexameric, barrel-stave pore in the membrane. However, steady-state and time-resolved fluorescence data indicate that the major membrane-bound species is a dimer on the bilayer surface (*34*), in agreement with previous molecular modeling (*35*). More recently, we proposed a kinetic mechanism (*15*) that provided a quantitative description of the binding and interaction of δ-lysin with phosphatidylcholine vesicles. This analysis suggested that δ-lysin crosses the bilayer as a short-lived trimer, with concomitant bilayer permeabilization, according to the sinking raft model. Here we revise some aspects of that analysis, further develop our model, and make a quantitative comparison of the experimental data for this peptide with the predictions of the different models. This analysis leads to a quantitative explanation of the mechanism of graded release by amphipathic peptides in general.

MATERIALS AND METHODS

Chemicals. POPC (1-palmitoyl-2-oleoyl-*sn*-glycero-3-phosphocholine) was purchased in a chloroform solution form Avanti Polar Lipids, Inc. U6 [4-(*N*,*N*-dimethyl-*N*-tetradecylammonium)methyl(7-hydroxycoumarin)chloride], 8-aminonaphthalene-1,3,6-trisulfonic acid, disodium salt (ANTS), and *p*-xylene bispyridinium bromide (DPX) were purchased from Molecular Probes. Carboxyfluorescein (99%) was from ACROS. Organic solvents p.A. were purchased from Merck. Lipids and probes were tested by TLC and used without further purification.

δ-Lysin. δ-Lysin (formyl-NH-Met-Ala-Gln-Asp-Ile-Ile-Ser-Thr-Ile-Gly-Asp-Leu-Val-Lys-Trp-Ile-Ile-Asp-Thr-Val-

[1] Abbreviations: PC, phosphatidylcholine; PE, phosphatidylethanolamine; PG, phosphatidylglycerol; PS, phosphatidylserine; DLPC, dilauroylphosphatidylcholine; DMPC, dimyristoylphosphatidylcholine; DPPC, dipalmitoylphosphatidylcholine; POPC, 1-palmitoyl-2-oleoylphosphatidylcholine; POPG, 1-palmitoyl-2-oleoylphosphatidylglycerol; NBD-DOPE, *N*-(7-nitrobenz-2-oxa-1,3-diazol-4-yl)dioleoylphosphatidylethanolamine; U6, 4-(*N*,*N*-dimethyl-*N*-tetradecylammonium)-methyl(7-hydroxycoumarin)chloride; LUV, large unilamellar vesicle; MLV, multilamellar vesicle; SUV, small unilamellar vesicle; P/L, peptide-to-lipid ratio.

Asn-Lys-Phe-Thr-Lys-Lys-COOH) was a gift from Dr. H. Birkbeck. Its purification was described previously (*15*, *36*). For the stopped-flow fluorescence measurements, lyophilized δ-lysin was dissolved in distilled water acidified to pH 3, to a final concentration of 200 μM, and stored frozen in 100 μL aliquots in Eppendorf tubes. Prior to being used, an aliquot was thawed and kept on ice. Immediately before an experiment, 5 μL of this solution was added to 1 mL of 0.10 M KCl (pH 3.0) to avoid changes in the concentration of δ-lysin in solution due to its tendency to stick to glass surfaces.

Preparation of Large Unilamellar Vesicles (LUVs). POPC solutions in chloroform were placed in a round-bottomed flask, and the solvent was rapidly evaporated using a rotary evaporator (Büchi R-114A) at 60 °C. The lipid film was then placed under vacuum for 5−8 h and hydrated by the addition of buffer to give a final lipid concentration of 10 mM. The suspension of multilamellar vesicles was subjected to five freeze−thaw cycles. It was then extruded 10 times through two stacked Nuclepore polycarbonate filters with a pore size of 0.1 μm, using a water-jacketed high-pressure extruder from Lipex Biomembranes Inc. The suspension was diluted in buffer to the desired concentration and used for fluorescence measurements. The buffer consisted of 20 mM MOPS (pH 7.5) containing 100 mM KCl, 0.01 mM EGTA, and 0.02% NaN_3. For experiments using fluorophores encapsulated in POPC vesicles, the lipid film was hydrated in 20 mM MOPS (pH 7.5), 0.01 mM EGTA, and 0.02% NaN_3, containing a KCl concentration adjusted to give the same osmolarity as 100 mM KCl. For carboxyfluorescein (50 mM), no KCl was needed; for ANTS and DPX (5 mM each), 70 mM KCl was included, and for DPX (45 mM), 30 mM KCl was included. Following extrusion, fluorophore-containing LUVs were passed through a Sephadex-G25 column to separate the dye in the external buffer from the vesicles. Lipid concentrations were assayed by the Bartlett phosphate method (*37*), modified as previously described (*15*), with the absorbance read at 580 nm.

Fluorescence Experiments. Steady-state fluorescence measurements (ANTS/DPX assay) were performed in an SLM-Aminco 8100 spectrofluorimeter. In the ANTS/DPX assay, which was performed as described in detail in refs *38* and *39*, excitation was at 365 nm (8 nm slit width) and emission was at 515 nm (16 nm slit width). The kinetics of the tryptophan (Trp) fluorescence change upon peptide dilution were followed with a Hi-Tech SF-61 stopped-flow fluorimeter. Samples were excited at 285 nm, and the fluorescence intensity was monitored by collecting Trp emission through a WG320 long-pass filter (Schott). The kinetics of carboxyfluorescein efflux or energy transfer between U6 and NBD were obtained using an SLM-Aminco 8100, or a Fluoromax, spectrofluorimeter, adapted with a RX2000 rapid kinetics spectrometer accessory (Applied Photophysics), equipped with an RX pneumatic drive accessory (Applied Photophysics). Carboxyfluorescein efflux was measured by the relief of self-quenching of fluorescence, measured by excitation at 470 nm and emission at 520 nm. In the experiments with fluorescence energy transfer between U6 and NBD, 1 mol % NBD-DOPE was codissolved with POPC, dried under vacuum, and hydrated in buffer to a final lipid concentration of 5 mM. After extrusion, NBD-DOPE in the outer membrane leaflet was reduced to a nonfluorescent derivative via incubation with dithionite, for 5 min, at a final concentration of 25 mM (*40*, *41*). Dithionite was removed from the external medium through gel filtration through a Sephadex-G25 column. U6 was added externally to the vesicles from a 0.50 mM stock solution in ethanol to a final concentration of 1% of the lipid in the outer monolayer of the vesicles, just prior to the kinetics experiment. U6 was excited at 350 nm, and NBD emission was recorded at 550 nm. All experiments were carried out at ambient temperature (approximately 22 °C).

Correction of Carboxyfluorescein Efflux for Quenching Effects. Because partially empty vesicles contribute to the fluorescence at later times, the theoretical kinetic curves were corrected for this contribution. This correction changes the calculated curves slightly; however, its effect on the fit parameter values is very minor. For a 100 μM suspension of LUVs, the volume inside the vesicles (V_i) is approximately 3.0×10^{-4} mL/mL of solution, assuming approximately spherical vesicles with a diameter of 100 nm. An estimate of 2.6×10^{-4} mL was made by Parente and Lentz (*42*). Let c_{in} and c_{out} be the concentrations of carboxyfluorescein inside and outside the vesicles, respectively. The quenching function is described well in ref *43*

$$Q(x) = 0.040 + e^{-0.0747x} \tag{1}$$

where x is the carboxyfluorescein concentration. Let CF(t) be the function that describes the increase in the level of carboxyfluorescein outside the vesicles. In the simplest case, this would be a simple exponential function

$$CF(t) = 1 - e^{-kt}$$

In general, it is a smooth function varying from 0 to 1. Then,

$$c_{in}(t) = c_{in}(0)\left\{[1 - CF(t)] + \frac{V_i}{V_o}\right\} \tag{2}$$

$$c_{out}(t) = \frac{V_i c_{in}(0) CF(t)}{V_o} \tag{3}$$

Now the fluorescence outside and inside the vesicles is

$$F_{out}(t) = Q[c_{out}(t)]c_{out}(t)V_o \tag{4}$$

$$F_{in}(t) = Q[c_{in}(t)]c_{in}(t)V_i \tag{5}$$

And the total fluorescence is

$$F(t) = F_{out}(t) + F_{in}(t)$$

$$F(t) = c_{in}(0)V_i\{Q[c_{out}(t)]CF(t) + Q[c_{out}(t)][1 - CF(t)]\} \tag{6}$$

The initial and final fluorescence values are thus

$$F(0) = c_{in}(0)V_i Q[c_{in}(0)] \tag{7}$$

$$F(\infty) = c_{in}(0)V_i Q[c_{in}(0)V_i/V_o] \tag{8}$$

Finally, the observed carboxyfluorescein fluorescence is

$$\frac{F(t) - F(0)}{F(\infty) - F(0)} = \frac{Q[c_{out}(t)]\mathrm{CF}(t) + Q[c_{out}(t)][1 - \mathrm{CF}(t)] - Q[c_{in}(0)]}{Q[c_{in}(0)V_i/V_o] - Q[c_{in}(0)]} \quad (9)$$

Model and Data Analysis. The experimental kinetic data were analyzed with the model depicted in Figure 2, which is slightly modified from our previous version (*15*). In the forward experiment, desorption from the inner leaflet into the vesicle interior was not included in the scheme because of the comparatively small magnitudes of the off-rate constants.

That scheme was translated into a set of coupled, nonlinear differential equations, which constitute the kinetic model. The following scheme is specific for a trimer as the inserted aggregate, but was appropriately modified for the other types of aggregates that were studied. All rate constants referring to solution processes are marked with an asterisk (e.g., k^*_{a1}), whereas constants without an asterisk refer to association with the membrane or processes on the membrane. In the following, T_w, D_w, and M_w are the concentrations of solution δ-lysin tetramers, dimers, and monomers, L represents the concentration of lipid vesicle, M_o and D_o represent the concentrations of monomers and dimers bound to the outer leaflet of the membrane, M_i and D_i represent the concentrations of monomers and dimers bound to the inner leaflet, respectively, and T_{ins} is the concentration of a trimer inserted in the lipid bilayer, which is the species responsible for dye efflux. Solution species:

$$\frac{dT_w}{dt} = -k^*_{d1}T_w + k^*_{a1}D_w^2 \quad (10)$$

$$\frac{dD_w}{dt} = 2k^*_{d1}T_w - 2k^*_{a1}D_w^2 - k^*_{d2}D_w + k^*_{a2}M_w^2 - k_{on2}LD_w + k_{off2}D_o \quad (11)$$

$$\frac{dM_w}{dt} = 2k^*_{d2}D_w - 2k^*_{a2}M_w^2 - k_{on1}LM_w + k_{off1}M_o \quad (12)$$

Outer-leaflet species:

$$\frac{dM_o}{dt} = k_{on1}LM_w - k_{off1}M_o + 2k_{d1}D_o - 2k_{a1}/(v_oL)M_o^2 - k_{in}/(v_oL)M_oD_o + k_{d2}T_{ins} \quad (13)$$

$$\frac{dD_o}{dt} = k_{on2}LD_w - (k_{off2} + k_{d1})D_o + k_{a1}/(v_oL)M_o^2 - k_{in}/(v_oL)M_oD_o + k_{d2}T_{ins} \quad (14)$$

$$\frac{dT_{ins}}{dt} = k_{in}/(v_oL)(M_oD_o + M_iD_i) - 2k_{d2}T_{ins} \quad (15)$$

Inner-leaflet species:

$$\frac{dM_i}{dt} = -2k_{a1}/(v_oL)M_i^2 + 2k_{d1}D_i - k_{in}/(v_oL)M_iD_i + k_{d2}T_{ins} \quad (16)$$

$$\frac{dD_i}{dt} = k_{a1}/(v_oL)M_i^2 - k_{d1}D_i - k_{in}/(v_oL)M_iD_i + k_{d2}T_{ins} \quad (17)$$

Carboxyfluorescein efflux:

$$\frac{d\mathrm{CF}_{out}}{dt} = k_{eflx}(1 - \mathrm{CF}_{out})T_{ins}/(v_oL) \quad (18)$$

Lipid flip-flop:

$$\frac{d[\mathrm{lipid}]_{in}}{dt} = k_{flip-flop}(0.5 - [\mathrm{lipid}]_{in})T_{ins}/(v_oL) \quad (19)$$

The apparent rate "constant" for insertion k_{in} depends on membrane curvature strain, which is itself caused by a difference in the concentrations of the peptide bound to the outer and inner leaflets of the lipid bilayer:

$$k_{in} = k_{a2}([\mathrm{P}]_{outer} - [\mathrm{P}]_{inner}) \quad \text{if } [\mathrm{P}]_{outer} > [\mathrm{P}]_{inner} \ (k_{in} = 0 \text{ otherwise}) \quad (20)$$

where $[\mathrm{P}]_{outer}$ and $[\mathrm{P}]_{inner}$ are the concentrations of peptide chains bound to the outer and inner leaflets of the bilayer, respectively, and k_{a2} is a true constant. The justification for eq 20 will be further developed in the Results. All concentrations, whether referring to solution species or membrane-bound species, are expressed relative to the total aqueous solution volume. Therefore, terms involving products of membrane-bound species are divided by the factor v_oL, where v_o ($\simeq$0.60/2) is the specific molar volume of the peptide on the membrane (0.60 M^{-1}), assuming a 15 Å average peptide width, divided by 2 to correct for the two leaflets of the lipid bilayer. For example, the concentration of bound monomer relative to the lipid (m_o) equals $M_o/(v_oL)$, M_o being its concentration relative to water. Initial concentrations were calculated from the rate constants. The sets of differential equations were solved by numerical integration with a fifth-order Runge−Kutta method with a constant step size (*44*). The numerical solution was directly fitted to the experimental data with a simplex algorithm. In the analysis of carboxyfluorescein efflux and lipid flip-flop, the rate constants (k^*_{a1}, k^*_{a2}, k^*_{d1}, and k^*_{d2}) and initial conditions obtained for the equilibria in aqueous solution were used as fixed parameters. The remaining rate constants (membrane association and self-association on the membrane) were adjusted by a global fit.

For the reverse experiment, an additional block of equations was added, corresponding to the initial state in the donor vesicles pre-equilibrated with δ-lysin. This block is similar to the block corresponding to association of δ-lysin with vesicles (eqs 13−17). The initial conditions were calculated from the integrated equations in the forward reaction setting the time to 15 min, which was the preincubation time of δ-lysin with empty vesicles.

For the analysis of lipid flip-flop experiments, it was necessary to determine the dependence of energy transfer efficiency on the concentrations of U6 and NBD-DOPE. This was done empirically by measuring the fluorescence intensity emitted by NBD at 550 nm upon excitation of U6 at 350 nm, as a function of the concentrations of both fluorophores uniformly incorporated in POPC LUVs. This concentration dependence is shown in Figure 1. It is apparent that, although

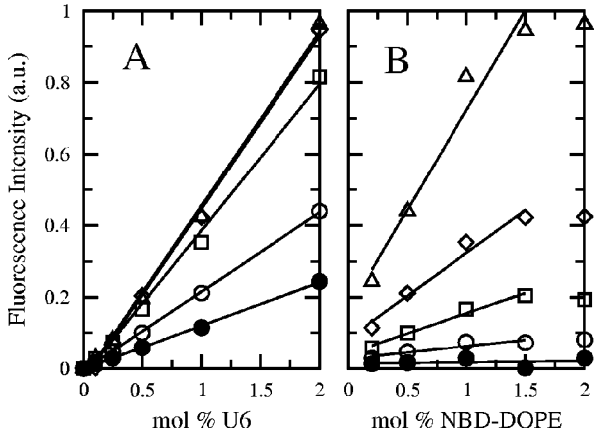

FIGURE 1: Empirical determination of the dependence of Förster (fluorescence) energy transfer between U6 and NBD-DOPE as a function of the concentration of the two fluorophores. U6 and NBD-DOPE were incorporated at concentrations between 0.2 and 2.0 mol % in POPC LUVs, and the fluorescence intensity was measured. Excitation of U6 was at 350 nm (U6), and emission of NBD was at 550 nm (NBD). (A) The NBD-DOPE concentration in POPC LUVs is fixed at 0.2 (●), 0.5 (○), 1.0 (□), 1.5 (◇), and 2.0 mol % (△), and the concentration of U6 is varied. (B) The U6 concentration in POPC LUVs is fixed at 0.2 (●), 0.5 (○), 1.0 (□), 1.5 (◇), and 2.0 mol % (△), and the concentration of NBD-DOPE is varied. This experiment shows that, to a reasonable approximation, energy transfer depends linearly on the concentration of both probes in the range of 0.2−1.5 mol %. This covers the range in which the two probes are used in the flip-flop experiment, in which each probe at 1 mol % was initially incorporated in the outer or inner leaflet of the bilayer.

a linear dependence of energy transfer efficiency on concentration is not to be expected in general, the dependence is approximately linear for the range used in this work (fluorophore concentration in the lipid of ≤1 mol %). Therefore, a linear dependence on the concentrations of both fluorophores was assumed in the equation used to fit the flip-flop kinetics data. For the concentrations of the lipid probes in the inner monolayer, we have (an identical equation applies to the outer monolayer)

$$\text{energy transfer}(t) = \text{constant} \times [\text{NBD}]_{\text{in}}(t)[\text{U6}]_{\text{in}}(t) \quad (21)$$

where the concentrations of NBD-DOPE and U6 are obtained from eq 19. It is assumed that the flip-flop rates are approximately the same for both fluorophores. It is not expected that the quality of the fits would improve significantly with addition of an extra parameter.

RESULTS

General Outline and Interpretation of the Kinetics. Several aspects of the interactions of δ-lysin with POPC LUVs were examined: (1) kinetics of peptide-induced efflux of initially entrapped carboxyfluorescein, (2) kinetics of peptide-induced lipid flip-flop, and (3) mechanism of peptide-induced dye release. The results have led to the proposal of the kinetic scheme shown in Figure 2 for interpreting the data globally. This scheme incorporates some simplifications and some essential modifications relative to our previous model (*15*), which are necessary to account for new observations. All kinetic data, which relate to δ-lysin aggregation in aqueous solution, carboxyfluorescein efflux from lipid vesicles induced by the peptide, and lipid flip-flop, can be understood with the same kinetic mechanism. Analysis of the kinetic

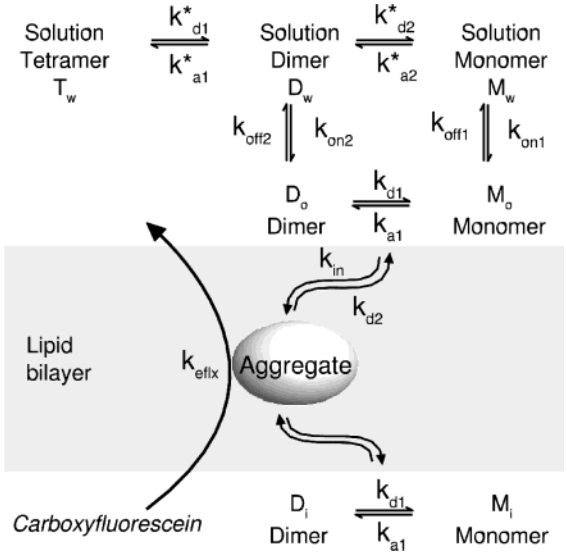

FIGURE 2: Kinetic mechanism of carboxyfluorescein efflux or lipid flip-flop induced by δ-lysin in POPC LUVs. The mathematical translation of this scheme is given by eqs 10−20. Lipid flip-flop follows the same scheme, except that the rate constant for efflux (k_{eflx}) is replaced by the rate constant for flip-flop ($k_{flip-flop}$).

data was performed by translating the scheme of Figure 2 into a set of coupled differential equations (eqs 10−19) that were solved numerically and globally fitted to the data. From this analysis, the membrane-inserted aggregate (Figure 2) appears to be a trimer or a tetramer. The lines shown in the figures along with the experimental results always represent the fits for a trimer model, which yielded the best fits. However, the fits to the tetramer model were not significantly worse. The rate constants for peptide self-association in solution were determined independently and used as fixed constants in the efflux and flip-flop analysis. The inserted aggregate is responsible for inducing both carboxyfluorescein efflux and lipid flip-flop. It acts as an enzyme that catalyzes these two "reactions". Other quantitative treatments have identified the time course of "pore" formation with dye efflux (*24*, *45*−*48*), which is not strictly correct. More accurately, the pore should be treated as a catalyst. Accordingly, the reaction and the rate equation for efflux or flip-flop should have the general form

$$X_{\text{in}} + P^* \rightleftharpoons X_{\text{out}} + P^*$$

$$\frac{dX_{\text{in}}}{dt} = -kP^*X_{\text{in}}$$

where P^* is the pore concentration in the membrane, X is the concentration of the entrapped dye or lipid that flips, and k is a bimolecular rate constant.

In what follows, we present, first, the results that establish the mechanism of dye release, second, the kinetic results that lead to the scheme of Figure 2, and, third, a physical interpretation of the kinetics.

Mechanism of Release of Fluorescent Dyes from POPC Vesicles. Although when P/L ≥ 1/200, the release of encapsulated dye (carboxyfluorescein) induced by δ-lysin from POPC vesicles is essentially complete, for smaller P/L dye release becomes incomplete. It was therefore important to investigate whether the release was graded or all-or-none because this provides valuable information about the mech-

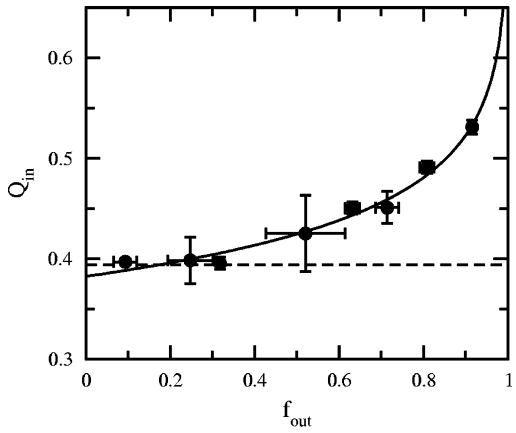

FIGURE 3: ANTS/DPX assay to determine the mechanism of release. The quenching function inside, $Q_{in} = F_i/F_i^{max}$, which is the ratio of ANTS fluorescence inside the vesicle in the presence (F_i) and absence (F_i^{max}) of quencher (DPX), is plotted against the ANTS fraction outside the vesicles, f_{out} (corrected for incomplete entrapment as described in ref *39*). The horizontal line would be the result expected for an all-or-none release. Release is clearly graded. The solid line represents a fit of eq 22 to the data points, which are averages and standard deviations from two separate samples. The fit parameters are as follows: $K_d = 50\ M^{-1}$, $K_a = 220\ M^{-1}$, and $\alpha = 0.22$.

anism of δ-lysin action. If a vesicle sample shows 50% release after peptide addition and release is graded, then all vesicles in that population have retained approximately half of the dye. But if release is all-or-none, half of the vesicles have released all of the dye, whereas the other half retained it entirely. The mechanism of leakage from POPC LUVs induced by δ-lysin was determined using the ANTS/DPX assay (*38*, *39*). In this method, a fluorophore (ANTS) and a quencher (DPX) are co-encapsulated in lipid vesicles and the degree of quenching inside the vesicles is monitored as a function of increasing concentrations of added peptide. If the mechanism of release is all-or-none, the degree of quenching inside is independent of peptide concentration because the contents of the vesicles that did not release anything remain unaltered. If the mechanism is graded, efflux of ANTS and DPX occurs and the fluorescence from the interior of the vesicles increases because quenching is a bimolecular process, which becomes less efficient as both ANTS and DPX become diluted. The results, shown in Figure 3, clearly indicate that release is graded. The data were corrected for incomplete entrapment (*39*) and analyzed according to ref 38. Equation 22, with the parameters given below, is the solid line represented in Figure 3:

$$Q_{in} = \frac{F_i}{F_i^{max}} = \frac{1}{[1 + K_d[DPX]_0(1 - f_{out})^{\alpha}][1 + K_a[DPX]_0(1 - f_{out})^{\alpha}]}$$

where F_i and F_i^{max} are the fluorescence intensities from the vesicle interior with and without quencher (DPX), respectively, $[DPX]_0$ (5 mM) is the initial concentration of DPX encapsulated (which is the same as $[ANTS]_0$ in our assay), f_{out} is the ANTS fraction outside the vesicles, K_d [50 M^{-1}; this value, given by Ladokhin et al. (*38*), coincides with our best fit] is the dynamic quenching constant, K_a (220 M^{-1}, best fit value) is the static quenching constant, and α (0.22, best fit value) is the ratio of the rates of release of DPX to ANTS, which indicates that DPX efflux is ~5 times faster than ANTS efflux. All-or-none efflux would correspond to a horizontal line in the plot.

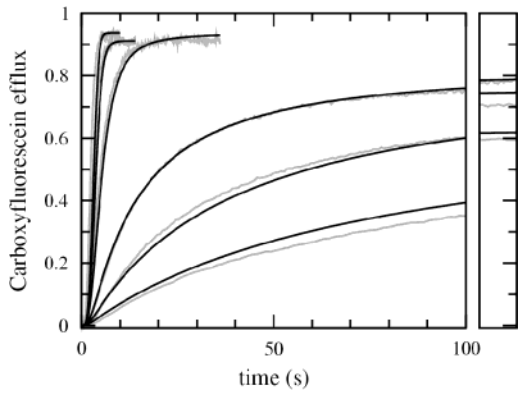

FIGURE 4: Kinetics of carboxyfluorescein efflux from POPC LUVs after addition of δ-lysin (0.5 μM). The curves, from left (fastest) to right (slowest), correspond to 25, 50, 100, 200, 300, and 400 μM lipid. The data were normalized by the Triton X-100 release levels. The lines represent the fits of the theoretical kinetic model to the experimental data. The curves are shown for the first 100 s. The last 10 s for the three slower curves are shown on the right (from top to bottom, 200, 300, and 400 μM lipid). The parameters for the global fit that is shown are as follows: $k_{a1} = 3.96 \times 10^3\ M^{-1}\ s^{-1}$, $k_{d1} = 13.7\ s^{-1}$, $k_{a2} = 1.57 \times 10^3\ M^{-2}\ s^{-1}$, $k_{d2} = 0.88\ s^{-1}$, $k_{on1} = 9.51 \times 10^3\ M^{-1}\ s^{-1}$, $k_{on2} = 3.46 \times 10^3\ M^{-1}\ s^{-1}$, $k_{off1} = 1.05 \times 10^{-2}\ s^{-1}$, $k_{off2} = 5.47 \times 10^{-6}\ s^{-1}$ (calculated), $k_{eflx} = 1.02 \times 10^3\ M^{-1}\ s^{-1}$, and $k_{eflx} = 7.00 \times 10^2\ M^{-1}\ s^{-1}$. The parameter values for dissociation and association in solution are given in Figure 7. Because Triton X-100 release levels have an uncertainty of ~10%, an amplitude factor between 0.9 and 1.05 was included. For the fits that are shown, the amplitude factor values are 0.936, 0.911, 0.941, 0.907, 1.04, and 1.04 for 25, 50, 100, 200, 300, and 400 μM lipid, respectively. The result of the same global fit is shown in Figures 5−7 for the reverse experiment, lipid flip-flop, and peptide dissociation in solution, respectively.

Kinetics of Carboxyfluorescein Efflux from POPC Vesicles: Forward Reaction. In our previous work (*15*), carboxyfluorescein efflux curves were normalized to the apparent final fluorescence level. However, we have now found that carboxyfluorescein release is essentially complete for high P/L, but not for low P/L ($\leq$1/400). Therefore, we have repeated the efflux kinetics experiments and normalized the curves to Triton X-100 release levels. δ-Lysin (to a final concentration of 0.5 μM) was mixed with POPC LUVs varying in concentration between 25 and 400 μM (in terms of lipid). Triton X-100 was added, to a final concentration of 1%, to dissolve the vesicles and give the maximum possible fluorescence level. The experimental results are the gray lines shown in Figure 4. The curves are sigmoidal (*15*), especially at high P/L (25 μM lipid). A strong dependence on lipid concentration is observed, the reaction becoming slower with an increasing lipid concentration, contrary to simple bimolecular kinetics. The reason is that the reaction rate increases with P/L, suggesting that binding of a critical number of peptides or their aggregation on the membrane is necessary for dye efflux to occur. A priori, the sigmoidal shape of the curve can arise for different reasons. It may reflect cooperativity in peptide aggregation (*49*), or it may indicate that several steps occur prior to the observable event (dye efflux) (*50*). Therefore, sigmoidicity is not a diagnostic

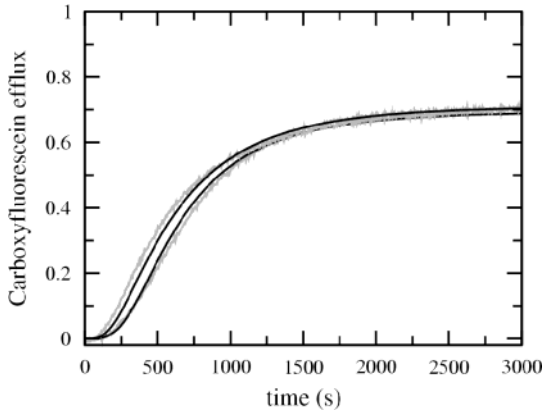

FIGURE 5: Reverse experiment of carboxyfluorescein efflux from POPC LUVs induced by δ-lysin. Donor vesicles were prepared by preincubating 1 μM δ-lysin with 100 or 460 μM POPC (empty LUVs) for 15 min, and the kinetics were followed after the samples were mixed with acceptor vesicles (containing dye) so that the final concentration of POPC was 250 μM in both cases The final δ-lysin concentration was 0.5 μM, after mixing, in the stopped-flow experiment. The efflux fraction is normalized to the Triton X-100 release level. The amplitude factors were 1.0 in both curves. The lines are the result of a global fit, with exactly the same parameters used in Figures 4, 6, and 7.

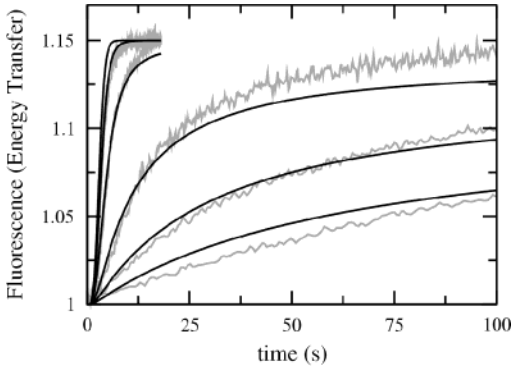

FIGURE 6: Kinetics of lipid flip-flop induced by δ-lysin in POPC LUVs. Förster energy transfer between U6 and NBD-DOPE was used to monitor lipid flip-flop. Initially, NBD-DOPE was incorporated only in the inner monolayer of POPC vesicles (treated with dithionite), and U6 was only in the outer monolayer (added externally from solution). When peptide is added to these asymmetric vesicles, the distributions of two fluorophores are randomized across the bilayer and the extent of energy transfer between them increases. The excitation of U6 was at 350 nm, and the emission of NBD at 550 nm was recorded. Experimental curves, in gray, correspond to the same set of different lipid concentrations as in Figure 4, from left (fastest) to right (slowest), 25, 50, 100, 200, 300, and 400 μM lipid. The data were normalized to the initial fluorescence. The peptide concentration was 0.5 μM (final). The lines are the result of a global fit, with exactly the same parameters used in Figures 4, 5, and 7.

by itself. The lines in Figure 4 show the global fits of the kinetic model with a trimer as the inserted aggregate (pore).

Kinetics of Carboxyfluorescein Efflux: Reverse Reaction. The rate of carboxyfluorescein efflux was also measured in a reverse reaction. That is, beginning with δ-lysin associated with POPC vesicles without the encapsulated dye, the kinetics were followed when those vesicles were mixed with carboxyfluorescein-containing vesicles. The final levels of dye release were determined by the Triton X-100 assay to be ~70%. This experiment is essential both for assessing the reversibility of the reaction and for estimating the back reaction rates (desorption from vesicles and dissociation of peptide aggregates). The forward reaction is all but insensitive to those back rates. More importantly, the forward dye efflux experiment alone does not permit us to distinguish between different aggregate numbers in the pore state. This distinction only becomes possible if the reverse reaction is also taken into account. The results are shown in Figure 5. The overall kinetics are much slower than in the forward reaction because they are now dominated by the slow dissociation of δ-lysin from the vesicles. The process is faster if P/L is smaller in the preincubation. The smooth lines are the global fits of the kinetic model.

Kinetics of Peptide-Induced Lipid Flip-Flop. Measurements of lipid flip-flop induced by amphipathic peptides reported in the literature typically yield characteristic times on the order of a few minutes. On this basis, we had assumed that this was a slow process compared to δ-lysin-induced dye efflux (*15*). Now, a direct assessment of lipid flip-flop in the presence of δ-lysin was obtained by measuring the level of Förster energy transfer (*51*) between two fluorophores, U6 and NBD-DOPE. Both fluorophores were initially incorporated, at concentrations of 1 mol % in the lipid. NBD-DOPE was restricted to the inner monolayer of the POPC vesicles, by inactivation of the NBD fluorophore on the outside by reduction with dithionite. U6 was added externally from solution, afterward; therefore, it was initially only in the outer monolayer. When peptide is added to these asymmetric vesicles, the distributions of two fluorophores are randomized across the bilayer and the level of energy transfer between them increases. Lipid flip-flop was found to be very fast (Figure 6), with the same rate as carboxyfluorescein efflux. The intrinsic lipid equilibration time in the absence of peptide is ~1 h (data not shown). We had previously reported data for energy transfer between Trp-15 of δ-lysin and U6 incorporated in the outer leaflet of POPC vesicles (*15*). Assuming slow lipid flip-flop, we had interpreted a decrease in the level of energy transfer with time as being indicative of the peptide moving away from the U6 probe. The results presented here show that the previous interpretation is not completely correct: the extent of energy transfer between U6 and Trp-15 decreases mainly as a consequence of net U6 flip-flop to the inner monolayer of the lipid vesicle, although there is also a contribution from peptide translocation. These flip-flop data can be fitted with our kinetic mechanism, with the exact same parameter values as the carboxyfluorescein efflux data, as shown by the smooth curves in Figure 6. The rate constants for lipid flip-flop and dye efflux are, in fact, the same.

Kinetics of Dissociation of δ-Lysin Aggregates in Aqueous Solution. δ-Lysin forms large aggregates in aqueous solution at high concentrations and mainly tetramers above and close to 1 μM (*30*), with further dissociation below this concentration (*30*, *34*). The dissociation kinetics of δ-lysin in aqueous solution reported here extend the number of initial peptide concentrations. δ-Lysin solutions (in 0.1 M KCl at pH 3.0) were diluted into equal volumes of buffer, in the stopped-flow apparatus, to final δ-lysin concentrations of 0.25, 0.30, 0.35, 0.40, 0.50, 0.75, and 1.0 μM. The results are shown in Figure 7, where the best simultaneous fit to the all data sets is shown by the smooth curves. Below a δ-lysin concentraiton of 1 μM, tetramers, dimers, and monomers are in equilibrium, according to eqs 10−12. The molecular rate

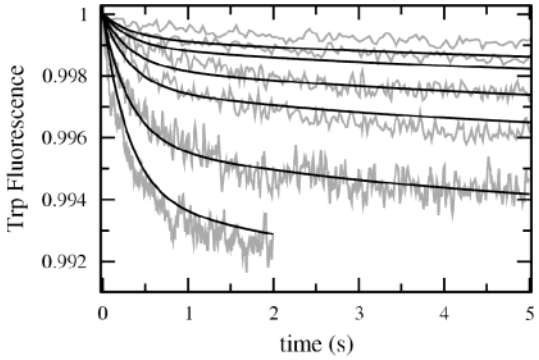

FIGURE 7: Dissociation of δ-lysin in aqueous solution. δ-Lysin solutions (in 0.1 M KCl at pH 3.0) were diluted into equal volumes of buffer in the stopped-flow apparatus to final δ-lysin concentrations of 0.25 (top curve), 0.30, 0.35, 0.40, 0.50, 0.75, and 1.0 μM (bottom curve). The data (in gray) show the intrinsic Trp fluorescence as a function of time, normalized to the initial fluorescence for each curve. The best simultaneous fit of eqs 10−12 to the all data sets is shown by the solid lines. The parameter values are as follows: $k^*_{d1} = 3.0\ s^{-1}$, $k^*_{a1} = 2.0 \times 10^5\ M^{-1}\ s^{-1}$, $k^*_{d1} = 8.0 \times 10^{-2}\ s^{-1}$, and $k^*_{a1} = 1.0 \times 10^5\ M^{-1}\ s^{-1}$. The data for the 0.25, 0.5, and 1.0 μM curves are from ref *15*.

Table 1: Rate Constants Derived from the Fits of the Model to the Experimental Data

Aqueous Solution	
k^*_{a1} ($M^{-1}\ s^{-1}$)	2×10^5
k^*_{d1} (s^{-1})	3
k^*_{a2} ($M^{-1}\ s^{-1}$)	1×10^5
k^*_{d2} (s^{-1})	8×10^{-2}

Binding to Vesicles		
	trimer	tetramer
k_{on1} ($M^{-1}\ s^{-1}$)	1×10^4	1×10^4
k_{off1} (s^{-1})	1×10^2	3×10^{-2}
k_{on2} ($M^{-1}\ s^{-1}$)	3×10^3	2×10^3
k_{off2}[a] (s^{-1})	3×10^{-6}	2×10^{-6}

Membrane		
	trimer	tetramer
k_{a1} ($M^{-1}\ s^{-1}$)	4×10^2	3×10^2
k_{d1} (s^{-1})	10	0.1
k_{a2} ($M^{-2}\ s^{-1}$)	2×10^3	2×10^3
k_{d2}[b] (s^{-1})	0.9	0.8
k_{eflx}[b] ($M^{-1}\ s^{-1}$)	1×10^3	1×10^3
$k_{flip-flop}$[b] ($M^{-1}\ s^{-1}$)	7×10^2	7×10^2

[a] k_{off2} was not fitted. It is determined by the thermodynamic cycle in Figure 2. [b] If k_{d2} and k_{eflx} are sufficiently large, there is a strong compensation between the two constants and only their k_{d2}/k_{eflx} ratio can be determined. Thus, the values shown here should be viewed only as approximate lower bounds for both k_{d2} and k_{eflx}.

constants for self-association and dissociation, obtained from the fits of the corresponding set of differential equations to the Trp fluorescence decay curves, are included in Table 1. Those values limit the number of parameters allowed to vary in the fit of the complete kinetic scheme to the carboxyfluorescein efflux data.

Kinetic Model and Quantitative Analysis of Data. Our data were quantitatively interpreted with the kinetic model shown in Figure 2. Table 1 indicates the order of magnitude estimates of the best parameters for both trimer and tetramer models. This new version of our model provides a simple but quantitative explanation for partial, graded dye release from lipid vesicles. We propose that dye efflux occurs

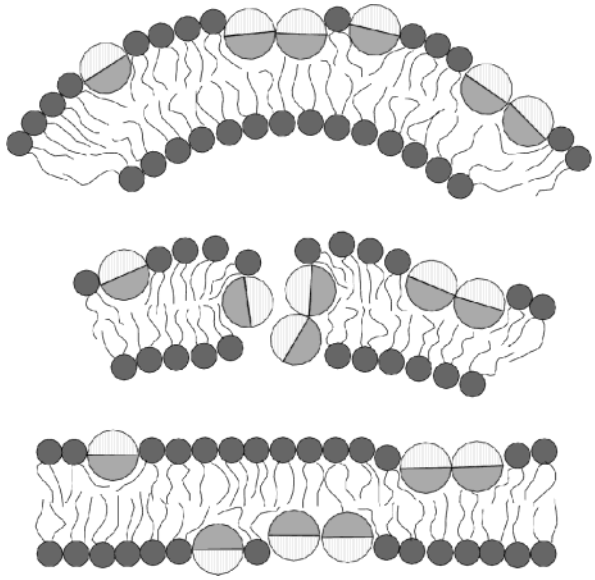

FIGURE 8: Sinking raft model for peptide-induced transient pore formation and peptide translocation across the lipid bilayer. The α-helices are shown as cross sections, the darker half-circles representing the hydrophobic faces and the lighter half-circles the polar faces. The polar angle for δ-lysin is 180°. Initially (top), binding of peptides creates a mass imbalance across the lipid bilayer with a consequent increase in local curvature. Some peptide self-association occurs, and the aggregate sinks deeper into the membrane (sinking raft). Transient higher aggregates form (trimers here) and perturb the bilayer, catalyzing both dye efflux and lipid flip-flop (center). As peptide translocation is completed, the mass balance across the bilayer is restored and the rate of efflux becomes very slow, leading to incomplete, graded efflux from the vesicle.

concomitantly with peptide translocation and that translocation takes place only if the bilayer is perturbed by a curvature strain. Because this curvature strain arises from a mass imbalance across the bilayer and because this mass imbalance is caused by the *bound* peptide itself (see Figure 8, top), we have postulated that the insertion specific rate, k_{in}, is not constant, but is given by (eq 20)

$$k_{in} = k_{a2}([P]_{outer} - [P]_{inner}) \quad \text{if } [P]_{outer} > [P]_{inner}\ (k_{in} = 0 \text{ otherwise})$$

where $[P]_{outer}$ and $[P]_{inner}$ are the concentrations of peptide chains bound to the outer and inner leaflets of the bilayer, respectively, and k_{a2} is a true constant. After initial binding from solution, the peptide concentration is larger in the outer monolayer, curvature strain increases, and peptide translocation and dye efflux are fast. Once equilibration of peptide concentrations inside and outside the vesicle is achieved, not only does the thermodynamic driving force (concentration difference) for translocation vanish but the insertion specific rate, k_{in}, also becomes zero, as the bound peptide concentration is also equal on both sides of the bilayer. The curvature strain disappears, and efflux stops. This is the explanation of graded release.

The kinetic model of Figure 2 is able to quantitatively describe all data sets with the same parameter values, which is nontrivial because these data correspond to four different types of experiments (Figures 4−7). The lines shown in those figures are the result of a global fit. The parameter set is given in Table 1. This set, however, is not unique because of some strong parameter compensation. The values given

in the table should be viewed as order of magnitude estimates for the rate constants. The exact values used in the fits shown are indicated in the legends of Figures 4 and 7. Various sets of models following the same general scheme were tried, varying the aggregate size and details of the individual steps. The fits are not very sensitive to fine details of the model, such as the number of intermediates preceding the effective pore or the exact order of the individual steps. On the other hand, estimation of aggregate size is quite robust. Models in which the transiently inserted state is a trimer or a tetramer fit the data very well globally. (Excellent fits can be obtained for individual curves if the parameters are allowed to deviate slightly from the best global fit values.) The trimer model fits slightly better than the tetramer, but the difference is not sufficient to discard the latter. However, with a dimeric or hexameric transient pore, it is not possible to obtain a good global fit. The forward efflux data alone could be fitted, but not together with the reverse reaction.

DISCUSSION

We have presented a quantitative analysis of dye efflux and lipid flip-flop kinetics induced by δ-lysin, an amphipathic, α-helical peptide. We have also demonstrated that the mechanism of dye release is graded. This allows us to significantly narrow the range of models that can be applied to peptide-induced leakage of vesicle contents, for the case of δ-lysin. The importance of a quantitative analysis in the selection or rejection of models is emphasized in this discussion.

Explanation of Graded Release from Vesicles. The problem of whether peptide-induced release of an encapsulated dye from phospholipid vesicles follows a graded or an all-or-none mechanism has been debated over the last 10 years. Release appears to be all-or-none for GALA (*24*), HNP-2 (*52*), pardaxin (*53*), a cecropin A-melittin hybrid (*54*), and, at a high P/L, viscotoxin A3 (*55*). Less clearly, indolicidin (from POPC) (*56*) and cecropin A (*57*) may also yield all-or-none release. The mechanism is graded for diphtheria toxin fragment A (*58*), reduced HNP-2 (*52*), mastoparan X (*48*, *59*), mastoparan (*Polistes*) (*59*), indolicidin (from POPG) (*56*), Ac-Trp-Leu_5 (*60*), and, at a low P/L, viscotoxin A3 (*55*). Initial data for melittin indicated all-or-none release (*61*), but later the mechanism was shown to be graded (*62*). The mechanism of all-or-none release is well understood (*24*): at a low P/L, some vesicles do not have enough peptides bound, thus preventing formation of a peptide aggregate required for pore formation. Dye release occurs from only those vesicles that contain a sufficient number of bound peptides. In contrast, graded release has not been well-understood. We propose that, in graded release, efflux of contents occurs while the membrane is under curvature strain, which arises because of an imbalance in the membrane-bound peptide concentration across the bilayer. Once equilibration is established, membrane curvature strain disappears, peptide translocation occurs at a negligible rate, and efflux stops. To the best of our knowledge, this is the first time that a plausible mechanism is shown to explain graded release quantitatively. An alternative explanation is that graded release would be a consequence of very slow pore formation. Using our quantitative model, this appears to be the only other way of obtaining incomplete dye release from one vesicle over a long time period. In this scenario, however, the fits to the experimental data are poor.

Implications for Models of Peptide Action. Let us note, first, that our type of analysis is not necessarily the only possible way of interpreting the kinetic data. It is possible that an altogether different type of model, for example, involving an even greater role for the lipid in communicating peptide interactions, in the absence of direct peptide contacts, could explain the observations reported here. What is clear is that for models that include bringing together a certain number of peptides in the membrane, an effective pore involving a transient trimer (or, at most, a tetramer) is consistent with the experimental kinetics of dye efflux and lipid flip-flop, whereas larger peptide assemblies are not. These results have important implications for the plausibility of several models commonly used to describe the mode of action of antimicrobial, α-helical, amphipathic peptides. The barrel-stave model is not compatible with graded dye release. Once formed, a number of barrel-stave pores remain embedded in the membrane, probably in dynamical equilibrium with monomers. This situation would always result in the complete release of vesicle contents, as long as a finite number of pores exist, which is in accordance with an all-or-none mechanism. Furthermore, the lipid flip-flop data argue strongly against the barrel-stave pore, although the model cannot be excluded on this basis alone. First, the barrel-stave should not perturb the membrane more than an integral membrane protein, which is not expected to enhance flip-flop as indicated by the effect of rhodopsin (*63*). Some synthetic hydrophobic peptides, such as those of the WALP and KALP families (*40*, *64*), do enhance lipid flip-flop, and are likely to be inserted in the membrane in the orientation proposed for the barrel-stave model. However, the characteristic time for flip-flop in the presence of those peptides is on the order of hours (*40*, *64*), whereas δ-lysin accelerates the process to a time scale of seconds. Second, and most importantly, the fact that dye efflux and lipid flip-flop occur with exactly the same rate strongly suggests that the two processes occur because of the same transient perturbation of the bilayer, as suggested previously by other researchers (*17*). There is no reason to expect that lipid flip-flop will correlate with the rate of dye flow through a channel type of pore, although we cannot absolutely exclude a fortuitous coincidence. In the carpet model, a large number of bound peptides is presumed to coat the outer leaflet of the bilayer, forming a "carpet", before membrane disruption occurs (*5*). This model is inconsistent with our results, first, because δ-lysin-induced carboxyfluorescein efflux promptly occurs even with only ∼20 peptides per vesicle (*15*) and, second, because the carpet model predicts that vesicle disruption leads to micellization, which is inconsistent with graded dye release. δ-Lysin does not induce vesicle micellization at a low P/L. This is true at least when the P/L < 1/50 in POPC (*15*), the P/L < 1/10 in DPPC (*31*), and the P/L < 1/60 in DMPC (*32*). In POPC, micellization should actually occur only at very large P/L values because chain unsaturation appears to protect lipid vesicles from peptide-induced micellization (*65*) or to reduce the efficiency of pore formation (*66*). The largest P/L reached in the experiments presented here is 1/50. Even if the carpet model is modified, removing the prediction of vesicle disintegration (micellization), establishing a peptide carpet would appear formally to be a

very large number of peptides in the aggregate in the kinetic model. But if, as we found, a hexamer aggregate is too large to fit the data, anything larger will not fit either. The two-state model (*16*, *19*, *20*) shares some of the same problems of the carpet model. It does not predict vesicle disintegration but simply that a "phase transition" occurs at a critical concentration of surface-bound peptides, from a parallel to a perpendicular orientation relative to the membrane surface. The model is inconsistent with our results because, if a collective reorientation were required, the effective aggregate size would be very large. Furthermore, the insertion would be a very low-probability event as soon as the surface peptide concentration becomes very small, whereas we observed relatively rapid efflux with as few as 20 peptides/vesicle. What appears to be consistent with these data is that a small aggregate forms, which is responsible for inducing both dye efflux and lipid flip-flop at the same rate. Moreover, this aggregate inserts in the membrane only transiently, as the peptide translocates to the inside of the vesicle. What remains to be understood is the structure of this transient pore.

Nature of the Pore. Two models for the peptide pore are compatible with these experimental observations. One is the toroidal hole model, originally proposed for magainin (*16*), and shown to be a transient structure (*67*−*69*). A peptide−lipid hole is formed with the peptides perpendicular to the membrane plane, generating a high-curvature region that enhances lipid flip-flop (*17*). Evidence for this type of holes has been produced by Huang and collaborators using oriented CD and neutron diffraction (*19*, *70*). However, those structures were obtained at large P/L values. Presumably, at a low P/L, they form only transiently (*67*−*69*). The question is whether the structures observed at very high P/L values are relevant to the low-P/L regime, which is probably the biologically relevant one. A second caveat is that it appears that the toroidal pore would require more than three to four peptides, which is the number deduced here for δ-lysin. To explain the small number of peptides involved in the transient pore, we have proposed the sinking raft model for a trimer (*15*). An updated version, including the effect of curvature strain induced by a mass imbalance across the bilayer, is shown in Figure 8. The peptides initially bind to the membrane and sink into the bilayer to an extent determined by their nonpolar angle, 180° for δ-lysin (Figure 8, top). The mass imbalance thus produced leads to increased curvature strain of the bilayer. This strain is relieved as the peptide is translocated to the inside (Figure 8, middle), in a process in which the lipid chains remain in contact with the hydrophobic face of the amphipathic α-helix. This perturbation causes both dye efflux and lipid flip-flop. Peptide translocation continues until equilibration across the membrane is established. In contrast to the toroidal pore model, the peptides maintain their long axes parallel to the membrane plane. This concept was first suggested precisely to account for the parallel orientation of cecropin A (*18*), indicated by infrared spectroscopy. An important modification of the model presented here relative to our original one is the role of the bilayer. The free energy of binding of the peptide to the membrane is first converted into bilayer strain. This perturbation allows the peptide to cross the hydrophobic interior of the membrane, which would normally be impermeable to such molecules. The role of lipid bilayer strain in peptide insertion and translocation has been proposed by other authors (*18*, *21*, *66*, *71*, *72*), but is invoked here to quantitatively explain graded release of vesicle contents. Recently, Binder and Lindblom (*22*) used a similar idea to explain the translocation of the Trojan peptide penetratin across the bilayer. Unlike δ-lysin, which has no charge, penetratin has an effective +5 charge. Instead of a mass imbalance, those authors invoke a charge imbalance that gives rise to an electric field across the membrane, which causes penetratin translocation through an "electroporation" type mechanism.

Most α-helical, amphipathic peptides remain largely oriented parallel to the membrane, at least at low P/L values (*16*, *18*, *20*, *21*, *73*, *74*), and appear to associate side by side (*15*, *18*, *34*, *75*). Recently, it was shown show that the peptide MSI-78, a magainin-2 analogue, not only inhibits the $L_\alpha \rightarrow H_{II}$ transition but also induces the formation of the H_I phase in POPC (*76*). Inhibition of the $L_\alpha \rightarrow H_{II}$ phase transition is usually taken as an indication that the peptides associate mainly with the headgroup region of the bilayer. This effect has been observed for magainin-2 (*12*) and six of its analogues (*77*). Furthermore, for the human antimicrobial peptide LL-37 specifically labeled with ^{15}N, the orientation of the $^{15}N-^{1}H$ bonds of the peptide bound to oriented lipid bilayers was determined by NMR (*21*). It was shown that LL-37 is always parallel to the membrane under a variety of conditions. The authors argue (*21*) that, between the barrel-stave, membrane micellization, and the toroidal hole model, the latter best explains their results. However, it appears to us that the sinking raft model not only is consistent with those results but even provides a more natural understanding.

ACKNOWLEDGMENT

We thank Dr. Harry Birkbeck for providing δ-lysin.

REFERENCES

1. Andreu, D., and Rivas, L. (1999) Animal antimicrobial peptides: an overview, *Biopolymers 47*, 415−433.
2. Bechinger, B. (1999) The structure, dynamics and orientation of antimicrobial peptides in membranes by multidimensional solid-state NMR spectroscopy, *Biochim. Biophys. Acta 1462*, 157−183.
3. Epand, R. M., and Vogel, H. J. (1999) Diversity of antimicrobial peptides and their mechanisms of action, *Biochim. Biophys. Acta 1462*, 11−28.
4. Matsuzaki, K. (1999) Why and how are peptide-lipid interactions utilized for self-defense? Magainins and tachyplesins as archetypes, *Biochim. Biophys. Acta 1462*, 1−10.
5. Shai, Y. (2002) Mode of action of membrane active antimicrobial peptides, *Biopolymers 66*, 236−248.
6. Zasloff, M. (2002) Antimicrobial peptides of multicellular organisms, *Nature 415*, 389−395.
7. Zasloff, M. (1987) Magainins, a class of antimicrobial peptides from *Xenopus* skin: isolation, characterization of two active forms, and partial cDNA sequence of a precursor, *Proc. Natl. Acad. Sci. U.S.A. 84*, 5449−5453.
8. Bessalle, R., Kapitkovsky, A., Gorea, A., Shalit, I., and Fridkin, M. (1990) All-D-magainin: chirality, antimicrobial activity and proteolytic resistance, *FEBS Lett. 274*, 151−155.
9. Wade, D., Boman, A., Wahlin, B., Drain, C. M., Andreu, D., Boman, H. G., and Merrifield, R. B. (1990) All-D-amino acid-containing channel-forming antibiotic peptides, *Proc. Natl. Acad. Sci. U.S.A. 87*, 4761−4765.
10. Matsuzaki, K., Sugishita, K., Fuiji, N., and Miyajima, K. (1995) Molecular basis for membrane selectivity of an antimicrobial peptide, magainin 2, *Biochemistry 34*, 3423−3429.
11. Matsuzaki, K., Nakamura, A., Murase, O., Sugishita, K., Fujii, N., and Miyajima, K. (1997) Modulation of magainin 2-lipid bilayer interactions by peptide charge, *Biochemistry 36*, 2104−2111.

12. Matsuzaki, K., Sugishita, K., Ishibe, N., Ueha, M., Nakata, S., Miyajima, K., and Epand, R. M. (1998) Relationship of membrane curvature to formation of pores by magainin 2, *Biochemistry 37*, 11856−11863.
13. Ehrenstein, G., and Lehar, H. (1977) Electrically gated ionic channels in lipid bilayers, *Q. Rev. Biophys. 10*, 1−34.
14. Dempsey, C. E. (1990) The actions of melittin on membranes, *Biochim. Biophys. Acta 1031*, 143−161.
15. Pokorny, A., Birkbeck, H., and Almeida, P. F. F. (2002) Mechanism and kinetics of δ-lysin interaction with phospholipid vesicles, *Biochemistry 41*, 11044−11056.
16. Ludtke, S. J., He, K., Heller, W. T., Harroun, T. A., Yang, L., and Huang, H. W. (1996) Membrane pores induced by magainin, *Biochemistry 35*, 13723−13728.
17. Matsuzaki, K., Murase, O., Fujii, N., and Miyajima, K. (1996) An antimicrobial peptide, magainin 2, induced rapid flip-flop of phospholipids coupled with pore formation and peptide translocation, *Biochemistry 35*, 11361−11368.
18. Silvestro, L., and Axelsen, P. H. (2000) Membrane-induced folding of cecropin A, *Biophys. J. 79*, 1465−1477.
19. Huang, H. W. (2000) Action of antimicrobial peptides: two-state model, *Biochemistry 39*, 8347−8352.
20. Ludtke, S. J., He, K., and Huang, H. W. (1994) Cooperative membrane insertion of magainin correlated with its cytolytic activity, *Biochim. Biophys. Acta 1190*, 181−184.
21. Henzler Wildman, K. A., Lee, D.-K., and Ramamoorthy, A. (2003) Mechanism of lipid bilayer disruption by the human antimicrobial peptide, LL-37, *Biochemistry 42*, 6545−6558.
22. Binder, H., and Lindblom, G. (2003) Charge-dependent translocation of the Trojan peptide penetratin across lipid membranes, *Biophys. J. 85*, 982−995.
23. DeGrado, W. F., Musso, G. F., Lieber, M., Kaiser, E. T., and Kezdy, F. J. (1982) Kinetics and mechanism of hemolysis induced by melittin and by a synthetic melittin analogue, *Biophys. J. 37*, 329−338.
24. Parente, R. A., Nir, S., and Szoka, F. C., Jr. (1990) Mechanism of leakage of phospholipid vesicle contents induced by the peptide GALA, *Biochemistry 29*, 8720−8728.
25. Fitton, J. E., Dell, A., and Shaw, W. V. (1980) The amino acid sequence of the delta haemolysin of *Staphylococcus aureus*, *FEBS Lett. 115*, 209−212.
26. Fitton, J. E. (1981) Physicochemical studies on delta haemolysin, a staphylococcal cytolytic polypeptide, *FEBS Lett. 130*, 257−260.
27. Kreger, A. S., Kim, K.-S., Zaboretzky, F., and Bernheimer, A. W. (1971) Purification and properties of staphylococcal delta hemolysin, *Infect. Immun. 3*, 449−465.
28. Dhople, V. M., and Nagaraj, R. (1993) δ-Toxin, unlike melittin, has only hemolytic activity and no antimicrobial activity: rationalization of this specific biological activity, *Biosci. Rep. 13*, 245−250.
29. Lee, K. H., Fitton, J. E., and Wüthrich, K. (1987) Nuclear magnetic resonance investigation of the conformation of δ-haemolysin bound to dodecylphosphocholine micelles, *Biochim. Biophys. Acta 911*, 144−153.
30. Thiaudière, E., Siffert, O., Talbot, J. C., Bolard, J., Alouf, J. E., and Dufourcq, J. (1991) The amphiphilic α-helix concept. Consequences on the structure of staphylococcal δ-toxin in solution and bound to lipids, *Eur. J. Biochem. 195*, 203−213.
31. Dufourc, E. J., Dufourcq, J., Birkbeck, T. H., and Freer, J. H. (1990) δ-Haemolysin from *Staphylococcus aureus* and model membranes. A solid-state ^{2}H-NMR and ^{31}P-NMR study. *Eur. J. Biochem. 187*, 581−587.
32. Lohner, K., Staudegger, E., Prenner, E. J., Lewis, R. N. A. H., Kriechbaum, M., Degovics, G., and McElhaney, R. N. (1999) Effect of staphylococcal δ-lysin on the thermotropic phase behavior and vesicle morphology of dimyristoylphosphatidylcholine lipid bilayer model membranes. Differential scanning calorimetry, ^{31}P nuclear magnetic resonance, Fourier transform infrared spectroscopy, and X-ray diffraction studies, *Biochemistry 38*, 16514−16528.
33. Mellor, I. R., Thomas, D. H., and Sansom, M. S. (1988) Properties of ion channels formed by *Staphylococcus aureus* δ-toxin, *Biochim. Biophys. Acta 942*, 280−294.
34. Talbot, J. C., Thiaudière, E., Vincent, M., Gallay, J., Siffert, O., and Dufourcq, J. (2001) Dynamics and orientation of amphipathic peptides in solution and bound to membranes: a steady-state and time-resolved fluorescence study of staphylococcal δ-toxin and its synthetic analogues, *Eur. Biophys. J. 30*, 147−161.
35. Raghunathan, G., Seetharamulu, P., Brooks, B. R., and Guy, H. R. (1990) Models of δ-hemolysin membrane channels and crystal structures, *Proteins 8*, 213−225.
36. Birkbeck, T. H., and Freer, J. H. (1988) Purification and assay of staphylococcal δ-lysin, *Methods Enzymol. 165*, 16−22.
37. Bartlett, G. R. (1959) Phosphorous assay in column chromatography, *J. Biol. Chem. 234*, 466−468.
38. Ladokhin, A. S., Wimley, W. C., and White, S. H. (1995) Leakage of membrane vesicle contents: determination of mechanism using fluorescence requenching, *Biophys. J. 69*, 1964−1971.
39. Ladokhin, A. S., Wimley, W. C., Hristova, K. W. C., and White, S. H. (1997) Mechanism of leakage of contents of membrane vesicles determined by fluorescence requenching, *Methods Enzymol. 278*, 474−486.
40. Kol, M. A., de Kroon, A. I., Rijkers, D. T., Killian, A., and de Kruijff, B. (2001) Membrane-spanning peptides induce phospholipid flop: a model for phospholipid translocation across the inner membrane of *E. coli*, *Biochemistry 40*, 10500−10506.
41. McIntyre, J. C., and Sleight, R. G. (1991) Fluorescence assay for phospholipid membrane asymmetry, *Biochemistry 30*, 11819−11827.
42. Parente, R. A., and Lentz, B. R. (1984) Phase behavior of large unilamellar vesicles composed of synthetic phospholipids, *Biochemistry 23*, 2353−2362.
43. Weinstein, J. N., Klausner, R. D., Innerarity, T., Ralston, E., and Blumenthal, R. (1981) Phase transition release, a new approach to the interaction of proteins with lipid vesicles. Application to lipoproteins, *Biochim. Biophys. Acta 647*, 270−284.
44. Press, W. H., Teukolsky, S. A., Vetterling, W. T., and Flannery, B. P. (1994) *Numerical Recipes in Fortran*, 2nd ed., Cambridge University Press, New York.
45. Arbuzova, A., and Schwarz, G. (1999) Pore-forming action of mastoparan peptides on liposomes: a quantitative analysis, *Biochim. Biophys. Acta 1420*, 139−152.
46. Schwarz, G., and Robert, C. H. (1990) Pore formation kinetics in membranes, determined from the release of marker molecules out of liposomes or cells, *Biophys. J. 58*, 577−583.
47. Schwarz, G., and Robert, C. H. (1992) Kinetics of pore-mediated release of marker molecules from liposomes or cells, *Biophys. Chem. 42*, 291−296.
48. Schwarz, G., and Arbuzova, A. (1995) Pore kinetics reflected in the dequenching of a lipid vesicle entrapped fluorescent dye, *Biochim. Biophys. Acta 1239*, 51−57.
49. Wyman, J., and Gill, S. J. (1990) *Binding and Linkage. Functional chemistry of biological macromolecules*, University Science Books, Mill Valley, CA.
50. Gutfreund, H. (1995) *Kinetics for the Life Sciences*, Cambridge University Press, New York.
51. Fairclough, R. H., and Cantor, C. R. (1977) The use of singlet−singlet energy transfer to study macromolecular assemblies, *Methods Enzymol. 48*, 347−379.
52. Wimley, W. C., Selsted, M. E., and White, S. H. (1994) Interactions between human defensins and lipid bilayers: evidence for formation of multimeric pores, *Protein Sci. 3*, 1362−1373.
53. Rapaport, D., Peled, R., Nir, S., and Shai, Y. (1996) Reversible surface aggregation in pore formation by pardaxin, *Biophys. J. 70*, 2502−2512.
54. Mancheno, J. M., Onaderra, M., Martinez del Pozo, A., Diaz-Achirica, P., Andreu, D., Rivas, L., and Gavilanes, J. G. (1996) Release of lipid vesicle contents by an antibacterial cecropin A-melittin hybrid peptide, *Biochemistry 35*, 9892−9899.
55. Coulon, A., Berkane, E., Sautereau, A. M., Urech, K., Rouge, P., and Lopez, A. (2002) Modes of membrane interaction of a natural cysteine-rich peptide: viscotoxin A3, *Biochim. Biophys. Acta 1559*, 145−159.
56. Ladokhin, A. S., Selsted, M. E., and White, S. H. (1997) Bilayer interactions of indolicidin, a small antimicrobial peptide rich in tryptophan, proline, and basic amino acids, *Biophys. J. 72*, 794−805.
57. Silvestro, L., Gupta, K., Weiser, J. N., and Axelsen, P. H. (1997) The concentration-dependent membrane activity of cecropin A, *Biochemistry 36*, 11452−11460.
58. Jiang, G. S., Solow, R., and Hu, V. W. (1989) Fragment A of diphtheria toxin causes pH-dependent lesions in model membranes, *J. Biol. Chem. 264*, 17170−17173.
59. Arbuzova, A., and Schwarz, G. (1996) Pore kinetics of mastoparan peptides on large unilamellar lipid vesicles, *Prog. Colloid Polym. Sci. 100*, 345−350.

60. Wimley, W. C., Hristova, K., Ladokhin, A. S., Silvestro, L., Axelsen, P. H., and White, S. H. (1998) Folding of β-sheet membrane proteins: a hydrophobic hexapeptide model, *J. Mol. Biol. 277*, 1091−1110.
61. Benachir, T., and Lafleur, M. (1995) Study of vesicle leakage induced by melittin, *Biochim. Biophys. Acta 1235*, 452−460.
62. Rex, S., and Schwarz, G. (1998) Quantitative studies on the melittin-induced leakage mechanism of lipid vesicles, *Biochemistry 37*, 2336−2345.
63. Wu, G. (1992) Studies on the photoreceptor disc membrane: lipid asymmetry, flip-flop, and electrostatic potential at specific sites on rhodopsin, Ph.D. Dissertation. University of California, Los Angeles.
64. Kol, M. A., van Laak, A. N. C., Rijkers, D. T. S., Killian, J. A., de Kroon, A. I. P. M., and de Kruijff, B. (2003) Phospholipid Flop Induced by Transmembrane Peptides in Model Membranes Is Modulated by Lipid Composition, *Biochemistry 42*, 231−237.
65. Monette, M., and Lafleur, M. (1996) Influence of lipid chain unsaturation on melittin-induced micellization, *Biophys. J. 70*, 2195−2202.
66. Nicol, F., Nir, S., and Szoka, F. C. (2000) Effect of phospholipid composition on an amphipathic peptide-mediated pore formation in bilayers vesicles, *Biophys. J. 78*, 818−829.
67. Matsuzaki, K., Murase, O., Tokuda, H., Funakoshi, S., Fujii, N., and Miyajima, K. (1994) Orientational and aggregational states in magainin 2 in phospholipid bilayers, *Biochemistry 33*, 3342−3349.
68. Matsuzaki, K., Murase, O., Fujii, N., and Miyajima, K. (1995) Translocation of a channel-forming antimicrobial peptide, magainin 2, across lipid bilayers by forming a pore, *Biochemistry 34*, 6521−6526.
69. Matsuzaki, K., Murase, O., and Miyajima, K. (1995) Kinetics of pore formation by an antimicrobial peptide, magainin 2, in phospholipid bilayers, *Biochemistry 34*, 12553−12559.
70. Yang, L., Weiss, T. M., Lehrer, R. I., and Huang, H. W. (2000) Crystallization of antimicrobial pores in membranes: magainin and protegrin, *Biophys. J. 79*, 2002−2009.
71. Huang, H. W. (1995) Elasticity of lipid bilayer interacting with amphiphilic helical peptides, *J. Phys. II 5*, 1427−1431.
72. Chen, F. Y., Lee, M. T., and Huang, H. W. (2002) Sigmoidal concentration dependence of antimicrobial peptide activities: a case study on alamethicin, *Biophys. J. 82*, 908−914.
73. Bechinger, B., Ruysschaert, J.-M., and Goormaghtigh, E. (1999) Membrane Helix Orientation from Linear Dichroism of Infrared Attenuated Total Reflection Spectra, *Biophys. J. 76*, 552a−563a.
74. Bechinger, B., Zasloff, M., and Opella, S. J. (1992) Structure and interactions of magainin antibiotic peptides in lipid bilayers: a solid-state nuclear magnetic resonance investigation, *Biophys. J. 62*, 12−14.
75. Wakamatsu, K., Takeda, A., Tachi, T., and Matsuzaki, K. (2002) Dimer structure of magainin 2 bound to phospholipid vesicles, *Biopolymers 64*, 314−327.
76. Hallock, K. J., Lee, D.-K., and Ramamoorthy, A. (2003) MSI-78, an analogue of the magainin antimicrobial peptides, disrupts lipid bilayer structure via positive curvature strain, *Biophys. J. 84*, 3052−3060.
77. Wieprecht, T., Dathe, M., Epand, R. M., Beyermann, M., Krause, E., Maloy, W. L., MacDonald, D. L., and Bienert, M. (1997) Influence of the angle subtended by the positively charged helix face on the membrane activity of amphipathic, antibacterial peptides, *Biochemistry 36*, 12869−12880.

BI0497087